Warm Molecular Gas in M51: Mapping H_2 Excitation and Mass with the Spitzer Infrared Spectrograph

Gregory Brunner[1,2]

Department of Physics and Astronomy, Rice University,

Houston, TX 77005

gbrunner@ipac.caltech.edu, gbrunner@rice.edu

Kartik Sheth[3], Lee Armus[3], and George Helou[3]

Caltech, Spitzer Science Center, Pasadena, CA 91125

Eva Schinnerer[4]

Max-Planck-Intitüt für Astronomie, Heidelberg, Germany

Stuart Vogel[5] and Mark Wolfire[5]

Department of Astronomy, University of Maryland, College Park, MD 20741

and

Reginald Dufour[1]

Department of Physics and Astronomy, Rice University, Houston, TX 77005

Received _____; accepted _____

[1]Department of Physics and Astronomy, Rice University, Houston, TX 77005

[2]Visiting Graduate Student Fellow, Spitzer Science Center, Caltech, Pasadena, CA 91125

[3]Spitzer Science Center, Caltech, Pasadena, CA 91125

[4]Max-Planck-Institüt für Astronomie, Heidelberg, Germany

[5]Department of Astronomy, University of Maryland, College Park, MD 20741

ABSTRACT

We have mapped the molecular gas in a radial strip across the disk of M51 using H_2 S(0) − H_2 S(5) pure rotational mid-infrared emission lines using the Infrared Spectrograph (IRS) on the Spitzer Space Telescope. The morphology of the molecular gas changes significantly in the different line maps. We find that the H_2 excitation temperature varies from 100 − 600 K across the galactic disk. The nucleus contains the hottest gas (T∼600 K) and the interarm regions have the coolest (T∼??) gas. We measured the H_2 mass surface density by modeling the gas distribution with a two temperature model: a warm (T = 100 − 300 K) phase using the low J lines and a hot phase (T = 400 − 600 K) using the high J lines. The hot phase gas surface density peaks at 0.24 $M_\odot/pc^2$ at the nucleus, wheras the warm gas phase surface density reaches a maximum of xx $M_\odot/pc^2$ in the north-eastern spiral arm. The spatial variation in the hot and warm phases indicates that the molecular gas is being heated by different excitation mechanisms in the nucleus and in the spiral arms. There are significant spatial offsets between the warm H_2 phase and the colder (∼ 10 K) H_2 gas traced by CO (J = 1 –0) emission, such that the warm H_2 is offset towards the downstream side of the cold gas. The warm H_2 emission is spatially coincident with Hα emission, indicating that the warm H_2 gas phase is primarily heated by the HII regions. In contrast the hotter H_2 emission is spatially coincident with [O IV](25.89 μm) and X-ray emission, indicating that shocks and/or X-rays are responsible for exciting this phase.

Subject headings: galaxies: ISM — galaxies: H_2 — galaxies: individual(M51)

1. Introduction

Star formation and galactic evolution are connected via the molecular gas in a galaxy. In the Milky Way, nearly all star formation occurs in molecular clouds (), although not all molecular clouds are actively forming stars. On a more global, galactic scale, star formation may be triggered whenever the molecular gas surface density is enhanced, for example, by a spiral density wave (), by increased pressure or gas density in galactic nuclei (;), due to hydrodynamic shocks along the leading edge of bars (;), and in the transition region at the ends of bars (;). How does this star formation affect the surrounding molecular gas? How is it heated and what is the distribution of the gas temperatures? How does the mass of the warm and hot gas vary from region to region? We address these questions using a spectral map of a radial strip across the spiral galaxy, M51.

M51 (also known as the Whirlpool galaxy and NGC 5194) is a nearby, face-on spiral galaxy that is rich in molecular gas. Its proximity (assumed to be 8.2 Mpc ()), face-on orientation, and grand-design spiral morphology make it the ideal target for many studies of the interstellar medium (ISM) across distinct dynamical, chemical, and physical environments in a galaxy. Studies of the molecular gas within M51 have revealed giant molecular associations (GMAs) along the spiral arms (), a reservoir of molecular gas associated with the nuclear AGN (), and star-formation in molecular clouds triggered by a spiral density wave (). In addition to being well-studied at millimeter and radio wavelengths, M51 has been also studied at X-ray, UV, optical, near-infrared, infrared, and submillimeter wavelengths (; **?**; ; ;). Here we present new mid-infrared spectra obtaineed with the Infrared Spectrograph (IRS) () on-board the *Spitzer Space Telescope*. Pure rotational emission lines of H_2 in the mid-infrared are powerful tools for observing the warmer (>100 K) phase of H_2 [1] The mid-infrared H_2 lines are important diagnostics of

[1]Although we are always exploring the warm phase of H_2, in this paper we always refer

the ISM because they allow us to model the H_2 excitation-temperature, mass (;), and ortho-to-para ratio (;). These quantitites, in turn, help us constraint the energy injection mechanism (i.e. radiative heating, shocks, turbulence) that heats the warm molecular gas phase in the ISM.

2. Observations and Data Reduction

2.1. Spectral Data

We mapped a radial strip across M51 using the short-low (SL) and long-low (LL) modules of the *Spitzer* IRS in spectral mapping mode. The radial strips were $324'' \times 57''$ and $295'' \times 51''$ in the SL and LL, respectively. Integration times in the SL and LL were 14.6 s. Each slit position was mapped twice and half-slit spacings were used. In total, 1,412 spectra were taken in the SL and 100 were taken in the LL (including background observations). Dedicated off source background observations were taken for the SL observations. Backgrounds for the LL observations were taken from outrigger data collected while the spacecraft was mapping in the adjacent module. The astronomical observation requests (AORs) are available on SST's Leopard and Spot (Project ID 200138, PI: K. Sheth).

The spectra were assembled from the basic calibration data (BCD) into spectral data cubes for each module using CUBISM (). Background subtraction and bad pixel removal was done within CUBISM. The individual IRS spectra were processed using the S14.0 version of the Spitzer Science Center (SSC) pipeline. In CUBISM, the SL and LL data cubes have $1.85''$ pixels and $5.08''$ pixels respectively. This pixel size is half the point spread

---

to a warm and hot phase corresponding to temperatures of, T = 100 − 300 K, and T = 400 − 1000 K respectively.

function (PSF) at the red end of the wavelength sampled by the modules. In principle, the PSF should vary with wavelength but since the PSF is undersampled at the blue end of the module, it is approximately constant across a given module. So the approximate resolution of the SL module is xx arcsecs and of the LL module is yy arcsecs. ** DELETE THAT COLUMN IN TABLE 1**

We created continuum subtracted line-only maps of the H_2 S(0) − H_2 S(5) using a combination of PAHFIT () and our own code. PAHFIT is a spectral fitting routine that decomposes IRS low resolution spectra with the main advantage being that it allows one to recover the full line flux of any blended features. Several H_2 lines are blended: the H_2 S(1) with the 17.0 μm PAH complex, H_2 S(2) with the [Ne II](12.8 μm), and the H_2 S(5) with the [Ar II](6.9 μm). We first concatenated SL1 and SL2, and LL1 and LL2 data cubes into two cubes, one for SL and one for LL. We smoothed each map in the cubes by a 3 × 3 pixel box, conserving the flux, to increase the signal-to-noise ratio of the spectra. Then, for each pixel, we extracted a spectrum and ran PAHFIT to decompose it. We saved the location of the pixel along with the PAHFIT output and reconstructed de-blended features and line maps for all of the mid-infrared features. In this paper we focus only on the H_2 line maps.

2.2. Ancillary Data: CO (J=1–0), Hα, and X-ray Observations

The BIMA (Berkely Illinois Maryland Array) CO (J = 1 −− 0) map was acquired as a part of the BIMA Survey of Nearby Galaxies (SONG) (;). At the distance of M51, the SONG beam ($5\farcs8 \times 5\farcs1$) subtends 220 pc × 190 pc. The Hα + [N II] image of M51 was observed at Kitt Peak as part of *Spitzer Infrared Nearby Galaxies Survey* (SINGS). The native pixel scale for that image is $0\farcs3$. Additional information about the Hα image can be found in the SINGS Fourth Data Release (DR4). X-ray emission from M51 was observed by the Advanced CCD Imaging Spectrometer (ACIS) on the *Chandra X-Ray Observatory* on

20 June 2000. The total integration time was 14,865 seconds. The resolution of the image is $\sim 1''$. Further details of the observations are presented in ().

3. Results

3.1. Morphology of H_2 Emission

*** MUST PUT A CROSS FOR THE NUCLEAR POSITION. ALSO CONVERT ALL JPGS TO *** EPS FOR SUBMISSION. KEEP THE JPGS THOUGH FOR TALKS / ETC. ALSO RENAME *** ALL FIGS to FIG1, FIG2 BECAUSE THIS IS THE FORMAT REQUESTED BY APJ.

We have detected and mapped H_2 emission from the six lowest pure rotational H_2 lines (Figure **??**). The maps reveal remarkable differences in the distribution of the H_2 emission in M51. H_2 S(0) emission is strongest in the northwest spiral arm peaking at an intensity of 3.66×10^{-18} W/m^2 and decreases by a factor of 2 in the nuclear region. In contrast, the H_2 S(1) emission peaks in the nucleus of the galaxy at an intensity of 1.03×10^{-17} W/m^2 and has an extension of equal intensity towards the northwest spiral arm. In the spiral arm itself, the H_2 S(0) peak is offset from the H_2 S(1) emission by $10\farcs2$ ($\sim$380 pc). These offsets cannot be explained by the difference in the resolution between the SL and LL map ** CHECK THIS BY SMOOTHING THE SL MAP TO LL RESOLUTION AND VERIFYING THAT THE TWO PEAKS ARE STILL DISTINCT. ** We find H_2 S(0) and H_2 S(1) emission as far as $5 - 6$ kpc from the nucleus of the galaxy. In the outer spiral arm, the H_2 S(0) intensity is a factor of 2 times lower than in the inner northwest spiral arm and the H_2 S(1) intensity is a factor of 5 times lower than in the nucleus.

** I SEE THAT YOU HAVE SEVERAL VERSIONS OF FIGURES AND I WOULD USE THE ** ONES WITH THE NUCLEAR CROSS AND LABEL ALL THE H2Sx FIGS

WITH THE ** SAME LABELS

The H_2 S(2) − H_2 S(5) maps show different molecular gas morphology within M51 through each H_2 line. The strongest H_2 S(2) emission is from the nucleus at 2.21 × 10^{-18} W/m^2. We also see bright H_2 S(2) emission from the inner northwest spiral arm at half the intensity of the nuclear peak. The H_2 S(3) peak at the nucleus is 1.35 × 10^{-17} W/m^2, a factor of ∼ 6 greater than the H_2 S(2) nuclear peak. There is also a linear bar-like structure in H_2 S(3) emission across the nucleus of the galaxy at a PA∼-10^0. The emission peaks in the H_2 S(2) and H_2 S(3) maps are not spatially coincident. For instance, in the inner spiral arm there is a H_2 S(2) peak coincident with the CO peak whereas the H_2 S(3)peaks further down the spiral arm. Offsets like these suggest that there may be variations in the excitation temperature from region to region within a galaxy, and even within a spiral arm.

The H_2 S(4) and H_2 S(5) lines are brightest at the nucleus with intensities of 3.05 and 8.04 × 10^{-18} W/m^2 respectively. The H_2 S(4) line shows emission in the nucleus and in the spiral arm to the west. In the spiral arm to the west of the nucleus, the H_2 S(4) intensity is 2.11 × 10^{-18} W/m^2. This is notable because the spiral arm to the southwest of the nucleus is very bright in CO and and studies have revealed very high molecular gas column densities in the southwest inner spiral arm (). H_2 S(5) emission is asymmetric in the nucleus and mimics the morphology of the H_2 S(3) line with extended emission to the north of the nucleus. The differences in the morphology of H_2 emission are indicative of changes in the H_2 excitation-temperature across the galaxy, which we discuss in the next section.

3.1.1. Note on Uncertainties in the H_2 *Line Intensity Maps*

** THIS SUBSECTION IS UNNECESSARY - WE DON"T HAVE A GOOD HANDLE ON ** IRS UNCERTAINTIES ANYWAYS AND THERE ARE SYSTEMATICS

THAT ARE NOT ** REALLY TAKEN INTO ACCOUNT HERE SO I RECOMMEND DELETING IT ENTIRELY **

The uncertainty in the H_2 line intensity varies as a function of line intensity across each map. The uncertainty in the H_2 S(0) line intensity ranges from $20 - 40$ % across the nuclear region and spiral arms. The uncertainty in the spiral arm intensity at greater distances from the center of the strip is $80 - 90$ %. The H_2 S(1) line map has lower uncertainties with the uncertainty being ~ 10 % in the nuclear region and $20 - 30$ % in the spiral arms. The H_2 S(2) and H_2 S(3) lines show similar uncertainties to each other. In the nuclear region their uncertainty is $10 - 30$ % and in the spiral arms their uncertainty is 50 $- 80$ %. The H_2 S(4) and H_2 S(5) lines only show emission from the nuclear region; their uncertainties in the line intensity are ~ 35 % and 25 %, respectively.

3.2. Mapping H_2 Excitation-Temperature and Mass across M51

3.2.1. Modeling H_2 Excitation-Temperature and Mass

The pure rotational lines of molecular hydrogen provide a powerful probe of the conditions of the ISM by placing constraints on the energy injection that excites H_2 (). Following ; we modeled the H_2 excitation and mass across M51.

First, we smoothed the H_2 S(1) $-$ H_2 S(5) maps were smoothed to the resolution of the H_2 S(0) map. The maps were then interpolated to the same spatial grid. Excitation diagrams across the strip were derived from the Boltzman equation using the formulation of Rigopoulou et al. (2002),

$$N_i/N = (g(i)/Z(\mathrm{T_{ex}}))exp(-T_i/\mathrm{T_{ex}}) \quad (1)$$

where $g(i)$ is the statistical weight of state i, $\mathrm{Z(T_{ex})}$ is the partition function, $\mathrm{T_i}$ is the

energy level of a given state, and T_{ex} is the excitation temperature. N and N_i are the total column density and the column density of a given state i and N_i is determined directly from the measured extinction-corrected flux by

$$N_i = 4\pi \times flux(i)/(\Omega A(i) h\nu(i)) \quad (2)$$

where A(i) is the Einstein A-coefficient, $\nu(i)$ is the frequency of state i, Ω is the solid angle of the beam, and h is Planck's constant. Table 1 lists the values for the wavelength, rotational state, Einstein A-coefficient, energy, and statistical weight of the pure rotational levels of H_2.

** PUT THE NAME OF THE REGION ON THE PLOTS. ALSO PUT THE NUMBERS OF ** THE TRANSITIONS ON ONE OF THEM. ** ALSO HOW DO I KNOW FROM THESE PLOTS THAT OPR = 3? YOU NEED TO SAY ** HERE THAT IF OPR =3 YOU EXPECT THE FOLLOWING IN THE BOLTZMANN ** DIAGRAM AND IF NOT THEN YOU EXPECT SUCH AND SUCH...

** OVERALL THIS PARA IS VERY CONFUSING. AT ONE POINT OPR IS 3 BUT ** SOMEHOW THIS ALSO SHOWS A RANGE OF TEMPERATURES? VERY CONFUSED. ** THIS NEXT PARAGRAPH REALLY NEEDS TO BE REWRITTEN.

In Figure **??** we present excitation diagrams from three different regions across the M51 strip. The excitation diagrams exhibit an ortho-to-para ratio (OPR) of 3 in the nuclear region. This is in agreement with the value of the OPR of the nuclear region determined by SINGS (). Outside the nucleus, the lower J (H_2 S(0) - H_2 S(3)) levels exhibit an OPR of 3. The H_2 S(4) measurement shows significant scatter in the excitation diagrams outside of the nuclear region of M51. This would indicate that the OPR is less than 3; however, due to the low signal-to-noise ratio of the H_2 S(4) map, we do not believe that the OPR determined

from the H_2 S(4) intensity reflects the OPR of the warm H_2. The excitation-diagrams also exhibit a change in slope as a function of rotational level. This indicates that a continuous distribution of H_2 temperatures is being sampled within the beam.

** REWRITE PARA ABOVE

** DO YOU ASSUME TEMPERATURES FIRST AND DRAW THE LINE OR GET A ** TEMPERATURE FROM THE LINES THEMSELVES? THAT WILL DETERMINE HOW THE ** NEXT PARA SHOULD START. HERE I AM ASSUMING YOU GET A BEST FIT TO ** THE HIGH J LINES AND CALL THAT YOUR TEMPERATURE. THEN SUBTRACT ** THAT CONTRIBUTION TO LOW J LINES AND THEN FIT A TEMP TO THOSE? ** CORRECT?

The simplest model beyond a single temperature model is a two temperature model, which we call a warm and hot phase from here on. To determine the hot phase temperature we do a least squares fit AT EVERY PIXEL? to the H_2 S(2) − H_2 S(5) lines. We subtract the contribution of this hot phase temperature from the lower J lines and do a least squares fit to the H_2 S(0) – H_2 S(2) lines. ** HOW DO YOU THEN GET THE MASS? **

3.2.2. Warm and Hot H_2 *Mass Distributions*

In Figure **??** we present the warm (*left*) and hot (*right*) H_2 mass distributions across the M51 strip[2] ** NO MAKE THE SIZES THE SAME AND DELETE THIS SENTENCE – Also note that the sizes of the plots of the warm and hot H_2 mass phases are different. **

** ITS BECOMING PAINFUL TO WRITE EVERYWHERE.. ARE YOU SURE

[2]Note that the non-rectangular shape of the strip is due to the offset between the SL and LL strips.

YOU ** NEED IT? WHY IS H_2 NOT SUFFICIENT - -SAME GOES FOR EVERY TIME ** YOU USE MATHRM ?? AND PLEASE REDEFINE COMMANDS SO YOU CAN USE A ** SHORTHAND NOTATION FOR COMMONLY USED LABELS., E.G. ** ** ** AT THE BEGINNING OF THE DOCUMENT.

The highest gas surface density for the warm H_2 phase is in the inner northwest spiral arm at 11 ** CHANGE ALL $PC^2 TOPC^{-2} ANDREMOVEDIVISIONSIGNS M_\odot$ pc^{-2} warm H_2. The gas surface density in the outer northwest and southeast spiral arms is maximum at the center of the spiral arms at 3.5 $M_\odot/pc^2$ and 1.0 $M_\odot/pc^2$ respectively. ** PEAKS CANNOT BE BIMODAL BY DEFINITON - I REWORDED THAT SENTENCE! The hot phase surface density is highest in the nucleus and interior to the inner spiral arm at 0.24 $M_\odot/pc^2$. The gas surface density of the hot phase in the spiral arms is 1/3–1/5th that of the nuclear region.

3.2.3. Warm and Hot H_2 *Excitation-Temperature Distributions*

** DO YOU MEAN MASS OR SURFACE DENSITY – PLEASE GET THE NOMENCLATURE ** CORRECT BASED ON THE UNITS YOU ARE USING. IF PER $PC^2 ITSHOULDBE **SURFACEDENSITY.$

** THIS SECTION NEEDS TO BE REWRITTEN. WRITE IT AS FOLLOWS. FIG XX ** AND YY SHOW IN GREYSCALE THE DISTRIBUTION OF TEMPERATURES ** DETERMINED FROM THE HIGH AND LOW TRANSITIONS AS DESCRIBED ABOVE. ** OVERLAID ON IT ARE CONTOURS OF THE H2 GAS SURFACE DENSITY. IN BOTH ** CASES WE FIND THAT THE TEMPERATURE AND GAS SURFACE DENSITY ARE ** INVERSELY CORRELATED. – THAT'S ALL YOU YOU NEED TO WRITE. YOU ** NEED TO REALLY UNDERSTAND WHY THE

INTERARM REGIONS HAVE SUCH HIGH ** TEMPS ACCORDING TO THIS FIGURE. IT REALLY CANNOT BE REAL BECAUSE ** OUR S/N IS LOWEST IN THESE REGIONS.

In Figure **??** we compare the warm H_2 mass distribution to the excitation-temperature. The gas is warmest in the nuclear region of M51 with the temperature ranging from $175 - 190$ K in the center of the galaxy. The gas is cooler within the spiral arms of M51 than in the inter-arm regions. The temperature in this spiral arm decreases from 175 K at the outer surface layers to 154 K in the most dense region of the arm indicating that the warm H_2 excitation-temperature is cooler at higher H_2 densities. In the outer northwest and southeast spiral arms (at $5 - 6$ kpc from the center of the galaxy each) molecular the gas excitation-temperature ranges from 150 K at the center to about 175 K near the edge of the spiral arms; again indicating that high density regions are cooler than low density regions.

The excitation-temperature distribution of the hot H_2 is shown in Figure **??** and reveals a different picture than the excitation-temperature distribution of the warm H_2. The excitation-temperature in the nuclear region ranges from 587 to 612 K. The excitation-temperature in the northwest inner spiral arm is the coolest at 538 K. The hottest excitation-temperatures are observed in the inter-arm regions where there is the least amount of H_2.

** I DON'T REALLY BELIEVE THIS –¿ DO YOU? YOU MAY BE MISLED BY THE ** LOW S/N IN THESE MAPS IN THE INTERARM REGION ESP. FOR THE HIGHEST J ** LINES. In contrast, in the southeast inter-arm region, the excitation temperature is in excess of 900 K.

4. Discussion

4.1. Comparison to Previous Studies of Warm and Hot H_2 in Galaxies

Previous studies have used aperture-averages over entire galactic nuclei to derive the physical conditions of the molecular gas (; ;). In M51, find that within the central 330 arcsec^2 (ADD PHYSICAL SCALE IN XX PC^2), the warm H_2 phase has a maximum temperature of 180 K and a total mass of $M_{warm} = 1.46 \times 10^6$ $M_\odot$. In the central 412 arcsec^2 of M51, we find a corresponding maximum of 186 K and a total mass of 1.63 $\times$ 10^6 $M_\odot$, consistent with the SINGS results. The SINGS team also measured the excitation-temperature of the hot phase (though they do not measure the mass in the hot phase) and find a hot H_2 excitation-temperature of 521 K. Over the same region, we find a maximum excitation-temperature of 584 K.

** BUT YOUR REAL STRENGTH IS THE SPATIAL RESOLUTION AND YOU SHOULD ** REALLY REWRITE THE TOP PARAGRAPH TO REFLECT THAT. SO SAY THAT WE ** HAVE THE ABILITY TO DO SPATIALLY RESOLVED STUDIES BUT IT WOULD BE ** GOOD TO COMPARE OUR NUMBERS TO THE AVERAGES FOUND BY PREVIOUS ** STUDIES. THEN SAY THAT THE SPATIALLY RESOLVED NUMBERS MATCH THE ** AVERAGED STUDIES SO MUCH SO THAT THE AVERAGED STUDIES MUST BE ** DOMINATED BY THE BRIGHTEST REGIONS.. OR IT COULD BE THAT YOU ARE ** AVERAGING THE NUMBERS YOU QUOTE ABOVE – IS THAT THE CASE? I AM ** CONFUSED A BIT HERE.

** I DON'T SEE THE POINT OF THE PARA YOU HAD HERE BELOW. I WOULD DELETE IT. In a survey of Seyfert galaxies, Rigopoulou et al. (2002) find that the warm-to-hot phase mass fraction varies between $5 \times 10^3 - 1 \times 10^6$. This is significantly higher than the warm-to-hot mass fraction (Figure **??**) than we measure within the central

412 arcsec^2 of M51, 14.8. To measure the hot H_2 mass, we use the H_2 S(2) − H_2 S(5) lines, whereas Rigopoulou et al. (2002) used the H_2 S(5) − H_2 S(7) lines. Thus, the hot H_2 phase that they measured is preferentially offset to higher H_2 excitation-temperatures and lower H_2 masses.

4.2. The Warm-to-Hot H_2 Mass Ratio

** NOW WE GO BACK TO DESCRIBING WARM VS. HOT? I THOUGHT WE WERE IN ** THE DISCUSSION SECRION HERE. THIS IS REPETITIOUS. DIDN'T YOU ** ALREADY DO THIS BEFORE? JUST REDUCE THE FOLLOWING PARA TO ONE ** LINE. SAY THAT THE WARM TO HOT RATIO VARIES (PERHAPS YOU CAN SHOW ** THE DIVISION OF THE TWO MAPS RATHER THAN OVERLAYING THEM WHICH DOES ** NOT CONVEY QUANTITATIVE INFO. YOU JUST NEED TO SAY THIS IS THE ** RATIO SEE...

In Figure **??**, we compare the warm H_2 mass distribution to the hot H_2 mass distribution. The warm H_2 mass distribution peaks at in the northwest inner spiral arm and the hot H_2 mass distribution peaks at in the nucleus and in the region interior to the northwest spiral arm. It is evident from the figure that the warm-to-hot H_2 mass ratio is not constant across the galaxy but is lowest in the nucleus of the galaxy (at 12) and increases to 170 and 136 in the southeast and northwest spiral arms, respectively. The differences between the warm and hot H_2 mass distributions and the variations in the morphology of M51 as a function of rotational energy level suggest different origins to the warm and hot H_2 phases and that the primary excitation mechanisms of the warm and hot H_2 phases differ.

** THEN IN THIS PARA JUST SAY - THE MOST OBVIOUS HEATING

MECHANISM FOR ** THE MOLECULAR GAS IS STAR FORMATION OR NUCLEAR ACTIVITY. THE FORMER ** CAN BE TRACED USING HALPHA AND HTE LATTER USING XRAYS AND OIV LINE. ** IT WOULD ALSO BE INTERESTING TO SEE HOW THE WARM GAS WAS ** DISTRIBUTED RELATIVE TO THE COLD GAS - SO WE ALSO COMPARE OUR DATA ** TO CO DATA FROM SONG.

In order to understand the H_2 excitation and where each excitation mechanism is dominant, we made comparisons of the H_2 line intensity and mass distributions to diagnostics of three excitation mechanisms: UV photons emitted in dense photon dominated regions (PDRs) and H II regions, shocks, and X-rays. We use CO (J = 1 − 0) emission to determine the location of the H_2 relative to locations dense PDRs, Hα imagery to identify H II regions (), [O IV](25.98 μm) line emission as a diagnostic of shocks (), and the 0.5 − 10.0 keV X-ray band to distinguish X-ray dominated regions (XDRs). The following section compares the H_2 mass distributions to CO (J = 1 - 0), Hα, [O IV], and X-ray emission.

4.3. Distinguishing the H_2 Excitation Mechanisms

** AS A GUIDE TO DECREASING THE VERBOSITY OF THE ARTICLE, TRY AND ** REDUCE THE NEXT THREE SUBSECTIONS TO THREE PARAGRAPHS OF NO MORE ** THAN 10 SENTENCES (AND NO CHEATING WITH RUN-ON SENTENCES). THIS ** WILL MAKE THIS PAPER MUCH MORE COMPACT AND TRACTABLE. I WILL TAKE ** OUT THE SALIENT SENTENCES FROM THE FIRST SUBSECTION HERE AND PUT ** THEM INSIDE *** - THESE OUGHT TO BE THE 10 SENTENCES OR LESS YOU ** FOCUS ON.

4.3.1. H_2 *Excitation by UV Photons from PDRs: Comparison of* H_2 *to CO Emission*

In star-forming regions, H_2 exists within the PDR and deep into the molecular cloud. ** Owing to a low dissociation energy of 4.5 eV, H_2 formation generally does not occur within a PDR until the radiation field becomes sufficiently weak. ** Understanding H_2 in PDRs and implementing H_2 into photoionization codes has become the emphasis of many theoretical models. Recent advances in the CLOUDY photoionization code have included H_2 and modeled the structure of star-forming regions while treating the H II region and PDR as one continuous cloud (;). Kaufman et al. (2006) used Starburst99/Mappings to model H_2 pure rotational line emission from PDRs to probe the conditions of dense PDRs in star-forming regions. ** They show that within galaxies, where the telescope beam size is generally kiloparsecs across, H_2 emission could serve to probe the surface layers of dense molecular clouds. **

** HERE ARE YOU SAYING THAT THERE IS NO H2 WHERE THERE IS CO?? THAT IS NOT RIGHT. PERHAPS YOU MEAN TO SAY CO TRACES THE COLD GAS WHERE NO MIDIR H2 EMISSION IS SEEN – BUT THERE IS H2 THERE? RIGHT? ** CO is found deep within a molecular cloud where the temperatures are too cold to excite H_2 emission. In these regions, CO is collisionally excited by the more abundant H_2 molecule. CO is connected to H_2 in star-forming regions because at the surface layers of the molecular clouds, H_2 is excited and CO emits dipole rotational lines due to heating by the ionizing radiation of newborn massive stars ().

In Figure **??**, we compare the warm (*left*) and hot H_2 (*right*) mass distributions to CO (J = 1 − 0) emission. The brightest CO emission is seen in the spiral arms where the greatest amounts of warm H_2 mass are also found. ** The most striking result is that in the inner spiral arms, we see that the CO is offset toward the nucleus from the warm H_2 mass. The offset between the peaks in CO and warm H_2 mass is $7\farcs2$ in the northwest spiral

arms and 5″ in the southeast spiral arms. We believe that these offsets are real with one possible explanation being that the H_2 is tracing the regions of active star-formation within the giant molecular associations. ** REDUCE ABOVE SENTENCES INSIDE ** I IN THIS PARA TO 2 SENTENCES

We compare CO to the hot H_2 mass distribution (Figure **??**, *right*) and we see that the hot H_2 mass is most abundant in the nuclear region, interior to the CO bright spiral arms. In northwest spiral arm, the hot H_2 mass is offset from the CO by 2.″6. We believe that the offsets between the CO and the hot H_2 mass are real, however, they are likely due to the dominance of other excitation mechanisms (shocks or X-rays) in the nuclear region of M51.

*** THIS PARA REALLY CONFUSED ME. WHAT IS BELIEVABLE AND WHAT IS NOT. *** WHAT IS THE CO DEPTH IS NOT SUFFICIENT. LET'S TALK ABOUT THIS *** OVER THE PHONE OR ICHAT

In Figure **??**, we compare the CO intensity to the H_2 S(0) − H_2 S(3) line intensity maps. We see that the H_2 S(0) contours trace the CO spiral arms with one notable difference being that we detect H_2 S(0) emission far (5 − 6 kpc) from the nucleus of M51, where there is no CO detected. The H_2 S(1) − H_2 S(3) contours also trace the CO spiral arms; however, within the spiral arms, the H_2 is not necessarily aligned with the CO. For example, in the comparison of H_2 S(3) to CO, we see that in the inner spiral arms, the H_2 contours trace the CO; however, within the northwest arm, we see that there is strong H_2 emission offset to the west by 9.″3 from the bright CO emission in the same spiral arm. The offsets between the peaks in H_2 and CO emission are not systematic in any direction.

** The CO intensity in the nucleus of the galaxy is much fainter than in the bright CO spiral arms. ** JUST SAYS CO -¿ COLD GAS AND NO COLD GAS IN NUCLEUS. ** This is interesting because H_2 S(1) − H_2 S(3) emission is brightest in the nucleus of M51 where H_2 emission from the higher J lines is likely due to more energetic processes such as

shock excitation and X-rays (which we discuss in §4.3.3 and §4.3.4).

4.3.2. H_2 *Excitation by UV Photons from H II Regions: Comparison of* H_2 *to H*α *Emission*

** SENTENCES LIKE THE FIRST FOUR BELOW ARE UNNECESSARY IN A PAPER! ** OKAY IN A THESIS BUT STILL MAKES A PAPER WAAAY TO VERBOSE. JUST ** STICK TO THE RELEVANT, IMPORTANT STUFF THAT IS ADDING TO THE ** SCIENCE. ONLY GIVE EXTRA INFO IF ABSOLUTELY NEEDED TO SET UP AN ** ARGUMENT.

** AGAIN REDUCE THIS SUBSECTION TO 10 SENTENCES AND 1 PARA ONLY. ** BOTTOM LINE IS YOU ARE SAYING WARM H2 NOT CORRELATED WITH HALPHA ** RIGHT? WHAT IS THE HALPHA WAS EXTINCTED? WHAT ABOUT PASCHEN ALPHA ** - IS THAT A BETTER CORRELATION?

H II regions are sites of recent massive star formation. They illuminate bright nebulae in distant galaxies and outline the spiral arms. H II regions emit prodigious amounts of UV radiation at energies $\geq$ 13.6 eV capable of exciting and ionizing H_2. Hα imagery is often used to identify and map H II regions in star-forming galaxies. Scoville et al. (2001) used Hα and Paα imagery to identify and characterize over 1,350 H II regions in M51. **

In Figure **??**, we compare the warm (*left*) and hot (*right*) H_2 mass distributions to Hα emission. In general, the warm and hot H_2 concentrations are not cospatial with the Hα emission regions in the spiral arms with the one exception being that the warm H_2 mass in the inner spiral arms appears to trace the Hα emission. The warm H_2 mass contours show that local peaks in H_2 mass are found within the dust lanes. An example of this is in the northwest spiral arms where we see the H_2 mass offset from the Hα spiral arms with local

peaks being found in the dust lanes.

In Figure **??**, we compare the H_2 S(0) − H_2 S(3) line intensity maps to Hα emission. Comparison of the H_2 S(0) map to Hα reveals that the strongest H_2 emission in the northwest and southeast inner spiral arms is coincident with Hα emission; however, the other H_2 S(0) spiral arms show the strongest emission in the dust lanes, offset from the Hα spiral arms. The largest offsets are seen in the southwest spiral arm where the H_2 S(0) emission is offset from the Hα spiral arm by $\sim 15''$ (560 pc). H_2 S(1) emission appears to follow the dust lanes and the H_2 S(1) intensity subsides into the Hα spiral arms. H_2 S(2) and H_2 S(3) emission is also found in the dust lanes; however, there are instances (such as in the southeast spiral arm) where the H_2 emission appear to be found straddling the dust lane and Hα spiral arm.

These results are in contradiction to a previous study of rovibrational H_2 line emission in Seyfert galaxies by Quillen et al. (1999) who used *HST* NICMOS to map the H_2(1-0)S(1) (2.121 μm) and H_2(1-0)S(3)(1.957 μm) lines in 10 Seyfert galaxies. They found that the H_2 emission is generally coincident with Hα emission and near the dust lanes (though offset from them). One explanation for this could be that the rovibrational lines trace a much hotter (1000 − 5000 K) molecular gas which can be found associated with H II regions whereas the cooler H_2 traced by the lowest pure rotational transitions is found in dense PDRs and molecular clouds associated with star forming regions.

4.3.3. H_2 *Excitation by Shocks: Comparison of* H_2 *to [O IV](25.89 μm) Emission*

** THIS SUBSECTION IS ACTUALLY WELL WRITTEN AND GETS TO THE POINT ** IMMEDIATELY - QUITE IN CONTRAST TO THE PREVIOUS TWO. SO TRY TO ** FOLLOW THIS MODEL. BUT IT IS STILL TOO LONG AND VERBOSE

SO CUT IT ** DOWN TO ONE PARA IF POSSIBLE.

The [O IV](25.89 μm) line can be excited in shocks (), the stellar winds of massive Wolf-Rayet stars (), or by an active galactic nucleus (AGN)(). Though the [O IV] line is blended with the [Fe II](25.99 μm) line in *Spitzer* IRS low resolution spectra, PAHFIT can deblend the two lines and in mapping the H_2 S(0) and H_2 S(1) line in the LL data cubes, we also mapped the [O IV] line.

In Figure **??**, we compare the [O IV] intensity to the warm (*left*) and hot (*right*) H_2 disributions. The [O IV] emission is brightest in the nuclear region at 8.75×10^{-18} W/m^2 and the peak is coincident with the nuclear peak in the mass of the hot H_2. [O IV] emission subsides from the nucleus to the inner spiral arm by 50 %. We resolve weaker [O IV] emission within the warm and hot H_2 spiral arms. The [O IV] intensity in the spiral arms is a factor of ~ 6 lower in the spiral arms than the peak intensity found in the nucleus.

The [O IV] emission within the nuclear region of M51 is likely due to the weak Seyfert II nucleus () and is possibly associated with shocked gas from the outflows of the AGN. The peak of the [O IV] emission coincides with the nuclear peak in hot H_2 mass indicating that the hot H_2 phase in the nuclear region of the galaxy is AGN or shock heated. With 2.43×10^5 M$_\odot$ of hot H_2 in the central 0.58 kpc^2, it is unlikely that the hot H_2 is fueling the central AGN, but is excited by the AGN or shocks produced by it. In the nuclear region we observe a factor of 12 times greater warm H_2 mass. The warm H_2 mass is much greater within the spiral arms than within the nucleus and the warm-to-hot mass ratio is lowest in the nuclear region where the [O IV] intensity is greatest. In the nuclear region, shocks appear to be a more efficient means to excite the hot H_2 phase than the warm H_2 phase.

4.3.4. H_2 *Excitation by X-rays: Comparison of* H_2 *to X-ray Emission*

M51 has been extensively studied in X-rays by ASCA (), Newton XMM (), and the Chandra X-ray Observatory (). These observations of M51 have revealed more than 80 X-ray sources. Candidates for these X-ray sources include neutron stars, black holes, supernova remnants (SN 1994I), and a low-luminosity AGN (;). X-ray emission from the nuclear region of M51 has been studied by Terashima and Wilson (2001). They observe X-ray emission from the nucleus, the extranuclear cloud (XNC, to the south of the nucleus), and the northern loop. A radio jet has been observed connecting the nucleus of M51 to the XNC in 6 cm imagery (). The jet emanates from the south of the elongated nucleus and is shock heating ISM.

In Figure **??**, we compare the smoothed 0.5 - 10 keV band X-ray image to the warm (*left*) and hot (*right*) H_2 mass distributions. The 0.5 - 10 keV band has been smoothed to the resolution of the warm and hot H_2 mass distributions and the nucleus, XNC, and northern loop are indistinguishable in the smoothed image. X-ray emission is most intense from the nucleus and decreases into the northwest spiral arm that contains the greatest H_2 mass. There appears to be very little connection between the 0.5 - 10 keV X-ray band and the warm H_2 mass distribution.

The peak in X-ray emission is coincident with the hot H_2 mass peak. The most intense 0.5 - 10 keV X-ray emission originates from the nucleus and is oriented north-to-south, similar to the [O IV](25.89 μm) emission. The peak in X-ray emission is located within the peak in hot H_2 mass suggesting that X-rays play an important role in exciting the hot H_2 phase. While there is a correlation between X-ray emission and the hot H_2 phase, H_2 excitation by X-rays cannot be distinguished from H_2 excitation by shocks.

We further investigate X-ray excited H_2 emission in M51 by comparing the $0.5 - 10.0$ keV X-ray band to the H_2 S(2) $-$ H_2 S(5) line intensity maps (Figure **??**). The H_2 S(2) $-$

H_2 S(5) line intensities all peak at the X-ray source within the nucleus. The X-ray source fits within the H_2 contours because the X-ray image resolution is slightly higher than the resolution of each of the H_2 maps.

The morphology of the nuclear H_2 emission appears to be correlated with the X-ray source. The H_2 S(2) intensity peaks around the X-ray nucleus and the intensity decreases to the south by 70 % in the southern XNC. The bar structure seen in the H_2 S(3) emission is aligned with X-ray emission from the nucleus, XNC, and northern loop. The H_2 S(3) intensity peaks between the X-ray nucleus and the XNC. To the north of the nucleus, the contours follow the X-ray loop. To the south of the nucleus (into the XNC), H_2 S(3) intensity decreases by 80 %. The H_2 S(4) and H_2 S(5) line intensities are highest in the nucleus which coincides with strong X-ray emission from the nucleus and XNC.

** SAME COMMENT ON SECTION ABOVE.. TOO VERBOSE. 1 PARAGRAPH PLEASE.

5. Conclusions

** WE CAN WORK ON THIS LATER. AGAIN NEED TO MAKE IT CONCISE.

We have spectrally mapped a strip across M51 using the *Spitzer* IRS low resolution modules. We used the spatially resolved spectra to map H_2 S(0) − H_2 S(5) line intensities across the strip. We find:

1. The morphology of H_2 emission in M51 varies with H_2 rotational level. H_2 S(0) emission is strongest in the spiral arms of the galaxy while the higher J transitions show the strongest emission towards the nucleus. The H_2 S(1) intensity is strongest in the nuclear region and in the northwest spiral arms, however, the peak in H_2 S(0) intensity in the

northwest spiral arm is offset from the peak in H_2 S(0) intensity by 10.″2. The H_2 S(2) and H_2 S(3) maps show H_2 emission in the nucleus, spiral arms, and inter-arm regions of M51 and bar structure aligned north-to-south is apparent in H_2 S(3) emission. H_2 S(4) and H_2 S(5) emission is resolved in the nuclear region of M51.

2. The different morphologies of H_2 emission in M51 indicate significant spatial variations in H_2 excitation-temperature and mass. Excitation diagrams reveal that the H_2 exists in a continuous distribution of temperatures across the galaxy. Using the low J lines to trace the warm (T = 100 − 300 K) H_2, we find that the warm H_2 excitation-temperature is highest in the nuclear region at 192 K and the warm H_2 mass peaks in the northwest inner spiral arm at a mass density of 11 $M_\odot/pc^2$. Using the higher J lines to trace the hot (T = 400 − 1000 K) H_2, we find that the hot H_2 excitation-temperature is lowest in the inner spiral arms (500 − 550 K) and increases to $\sim$ 600 K in the nucleus, where the largest hot H_2 mass densities are found to be 0.24 $M_\odot/pc^2$.

3. The warm and the hot H_2 mass distributions are not cospatial and the warm-to-hot mass ratio varies across M51. The hot mass distribution shows two peaks, one in the nucleus of M51 and one located interior to the northwest inner spiral arm of M51. The warm mass distribution peaks in the northwest spiral arm and is offset from the hot mass peak by 11.″4. The warm-to-hot mass ratio varies across the galaxy with the ratio being $\sim$ 15 in the nucleus and increasing to $>$ 100 in the spiral arms. Variations in the warm-to-hot H_2 mass ratio and differences in the morphology of the H_2 emission across M51 indicate that the primary excitation mechanism differs for the warm and hot H_2 mass phases as a function of location within the galaxy.

4. CO emission is offset from the warm H_2 mass in the inner spiral arms of M51. These apparent offsets are real and are possibly associated with the regions of active star formation within the molecular clouds. In the spiral arms, the H_2 S(0) − H_2 S(3) contours trace the CO; however, within the spiral arms, the peaks in H_2 can be offset from the peaks in CO intensity. In the nucleus, the H_2 S(1) − H_2 S(3) lines are brightest and the CO intensity is a factor of ~ 2.5 weaker than in the spiral arms suggesting that H_2 emission from the higher J lines is excited by shocks of X-rays.

5. Comparing the distributions of H_2 to Hα reveals that the warm and hot H_2 mass is found in the dust lanes rather than at or around the Hα emission regions with the one exception being that the warm H_2 mass in the inner spiral arms is coincident with bright Hα emission. This is in contradiction to previous studies of spatially resolved rovibrational H_2 line emission in Seyferts that found the H_2 emission to be coincident with the Hα emission.

6. The peaks in [O IV](25.89 μm) intensity and and X-ray intensity are both coincident with the peak in hot H_2 mass in the nucleus of M51 suggesting that the hot H_2 in the nucleus is primarily excited by the AGN, shocks (possibly associated with the AGN), or X-rays associated with the AGN. The spatial distributions of the [O IV] emission and X-ray surface brightness are very similar, but a primary excitation mechanism (shocks or X-rays) of the hot H_2 mass phase cannot be distinguished. Further comparison of the H_2 S(2) − H_2 S(5) intensity maps to the X-ray surface brightness reveal that the nuclear H_2 emission is associated with X-rays and the bar structure apparent in the H_2 S(3) map is aligned with

the nucleus, XNC, and northern loop.

The author graciously acknowledges the Spitzer Science Center Spitzer Visiting Graduate Student Fellowship program and committee for providing support for this research. The author would like to specifically acknowledge the program coordinators, Phil Appleton and Alberto Noriega-Crepso. The author would also like to thank JD Smith for swift responses to questions about PAHFIT and CUBISM and Nicolas Flagey for productive discussions about PAHFIT. Partial support for the completion and preparation for publication of this study by the author was provided by AURA grant GO10822.1 to Rice University.

Facilities: Spitzer Science Center (SSC), Spitzer Space Telescope (SST), Berkely-Illinois-Maryland Array (BIMA).

REFERENCES

Aalto, S., Huttemeister, S., Scoville, N.Z., and Thaddeus, P., 1999, AJ, 522, 165

Abel, N.P., Ferland, G.J., Shaw, G., and van Hoof, P.A.M., 2005, ApJS, 161, 65

Allen, R.J., Heaton, H.I., and Kaufman M.J., 2004, ApJ, 608, 314

Blitz, L., 1995, SSR, 684

Calzetti, D. et al., 2005, ApJ, 633, 871

Carpenter, J.M. and Sanders, D.B., 1998, AJ, 116, 1856

Crane, P.C. and van der Hulst, J.M., 1992, AJ, 103, 1146

Dewangn, G.C., Griffiths, R.E., Choudhury, M., Miyaji, T., and Schurch, N.J., 2005, ApJ, 635, 198

Ford, H.C., Crane, P.C., Jacoby, G.H., Lawrie, D.G., and van der Hulst, J.M., 1985, ApJ, 293, 132

Helfer, T.T., Thornley, M.D., Regan, M.W., Wong, T., Sheth, K., Vogel, S.N., Blitz, L., and Bock, D.C.J., 2003, ApJS, 145, 259

Higdon, S.J.U., Armus, L., Higdon, J.L., Soifer, B.T., and Spoon, H.W.W., 2006, ApJ, 648, 323

Houck, J.R. et al., 2004, ApJS, 145, 18

Immler, S., Wilson, A.S., and Terashima, Y., 2002, ApJ, 573, L27

Kaufman, M.J., Wolfire, M.G., and Hollenbach, D.J., 2006, ApJ, 644, 283

Lord, S.D. and Young, J.S., 1990, ApJ, 356, 135

Lutz, D., Kunze, D., Spoon, H.W.W., and Thornley, M.D., 1998, A&A, 333, L75

Kennicutt, R.C. et al., 2003, PASP, 115, 928

Kenny, J.D.P. and Lord, S.D., 1991, ApJ, 381, 118

Matsushita, S. et al., 2004, ApJ, 616, L55

Neufeld, D.A., Melnick, G.J., and Harwit, M., 1998, ApJ, 506, L75

Neufeld, D.A., Melnich, G.J., Sonnentrucker, P., Bergin, E.A., Green, J.D., Kim, K.H., Watson, D.M., Forrest, W.J., and Pipher, J.L., 2006, ApJ, 649, 816

Palumbo, G.G.C., Fabbiano, G., Fransson, C., and Trinchieri, G., 1985, ApJ, 298, 259

Quillen, A.C., Alonso-Herrero, A., Rieke, M.J., Rieke, G.H., Ruiz, M., Kulkarni, V., 1999, ApJ, 527, 696

Regan, M.W., Thornley, M.D., Helfer, T.T., Sheth, K., Wong, T., Vogel, S.N., Blitz, L., and Bock, D.C.J., 2001, ApJ, 561, 218

Rigopoulou, D., Kunze, D., Lutz, D., Genzel, R., and Moorwood, A.F.M., 2002, A&A, 389, 374

Roussel, H. et al., 2007, in press

Schaerer, D. and Stasinska, G., 1999, A&A, 345, L17

Scoville, N.Z. and Young, J.S., 1983, AJ, 265, 148

Scoville, N.Z., Yun, M.S., Armus, L., and Ford, H., 1998, ApJ, 493, L63

Scoville, N.Z., Polletta, M., Ewald, S., Stolovy, S.R., Thompson, R., and Rieke, M., 2001, AJ, 122, 3017

Shaw, G., Ferland, G.J., Abel, N.P., Stancil, P.C., and van Hoof, P.A.M., 2005, ApJ, 624, 794

Sheth, K., Regan, M.W., Vogel, S.N., and Teuben, P.J., 2000, ApJ, 532, 221

Sheth, K., Vogel, S.N., Regan, M.W., Tueben, P.J., Harris, A.I., and Thornley, M.D., 2002, AJ, 124, 2581

Sheth, K., Vogel, S.N., Regan, M.W., Thornley, M.D., and Teuben, P.J., 2005, ApJ, 632, 217

SINGS: The Spitzer Infrared Nearby Galaxies Fouth Data Delivery, May 2006.

Smith, J.D.T. et al., 2004, ApJS, 154, 199

Smith, J.D.T. et al., 2007, ApJ, 656, 770

Terashima, Y., Ptak, A., Fujimoto, M.I., Kunieda, H., Makishima, K., and Sherlemitsos, P.J., 1998, ApJ, 496, 210

Terashima, Y. and Wilson, A.S., 2001, ApJ, 560, 139

Tully, R.B. 1988, Nearby Galaxies catalog (Cambridge:Cambridge University Press)

Vogel, S.N., Kulkarni, S.R., and Scoville, S.Z., 1988, Nature, 334, 402

Young, J.S. and Devereux, N.A., 1991, ApJ, 373, 414

Young, J.S. and Scoville, N.Z., 1991, ARA&A, 29, 581

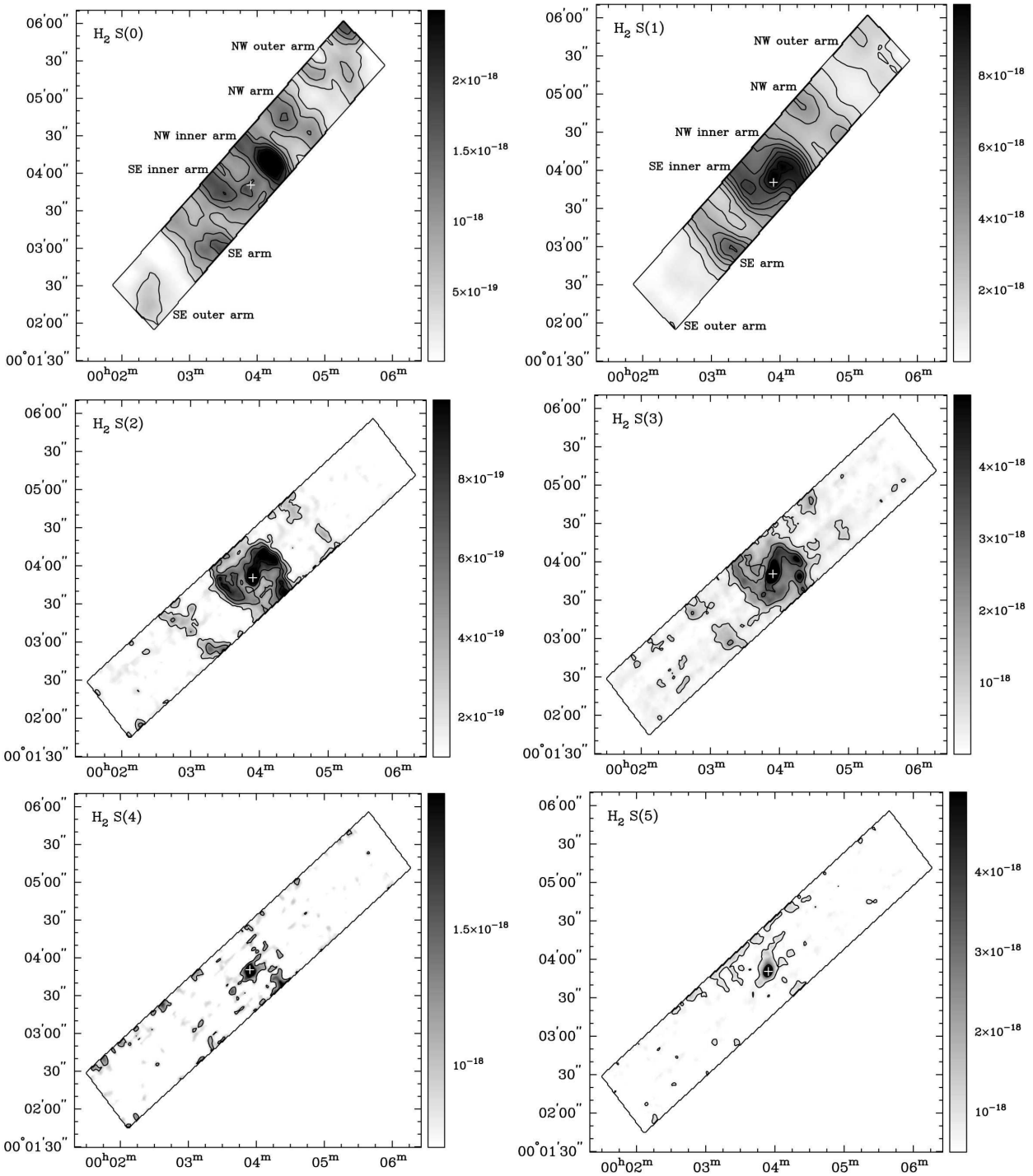

Fig. 1.— Maps of the H_2 S(0) (*top left*), H_2 S(1) (*top right*), H_2 S(2) (*middle left*), H_2 S(3) (*middle right*), H_2 S(4) (*bottom left*), and H_2 S(5) (*bottom right*) intensity across the SL and LL strips that we mapped with the Spitzer IRS. The H_2 S(0) and H_2 S(1) maps are created from the LL data cubes. The H_2 S(2), H_2 S(3), H_2 S(4), and H_2 S(5) maps are created from the SL data cube. The grey-scale is in units of W/m^2. Contour levels are at 2.9 $\times$ 10^{-18}, 2.2 $\times$ 10^{-18}, 1.8 $\times$ 10^{-18}, 1.5 $\times$ 10^{-18}, 1.1 $\times$ 10^{-18}, 7.3 $\times$ 10^{-19}, and 3.7 $\times$ 10^{-19}

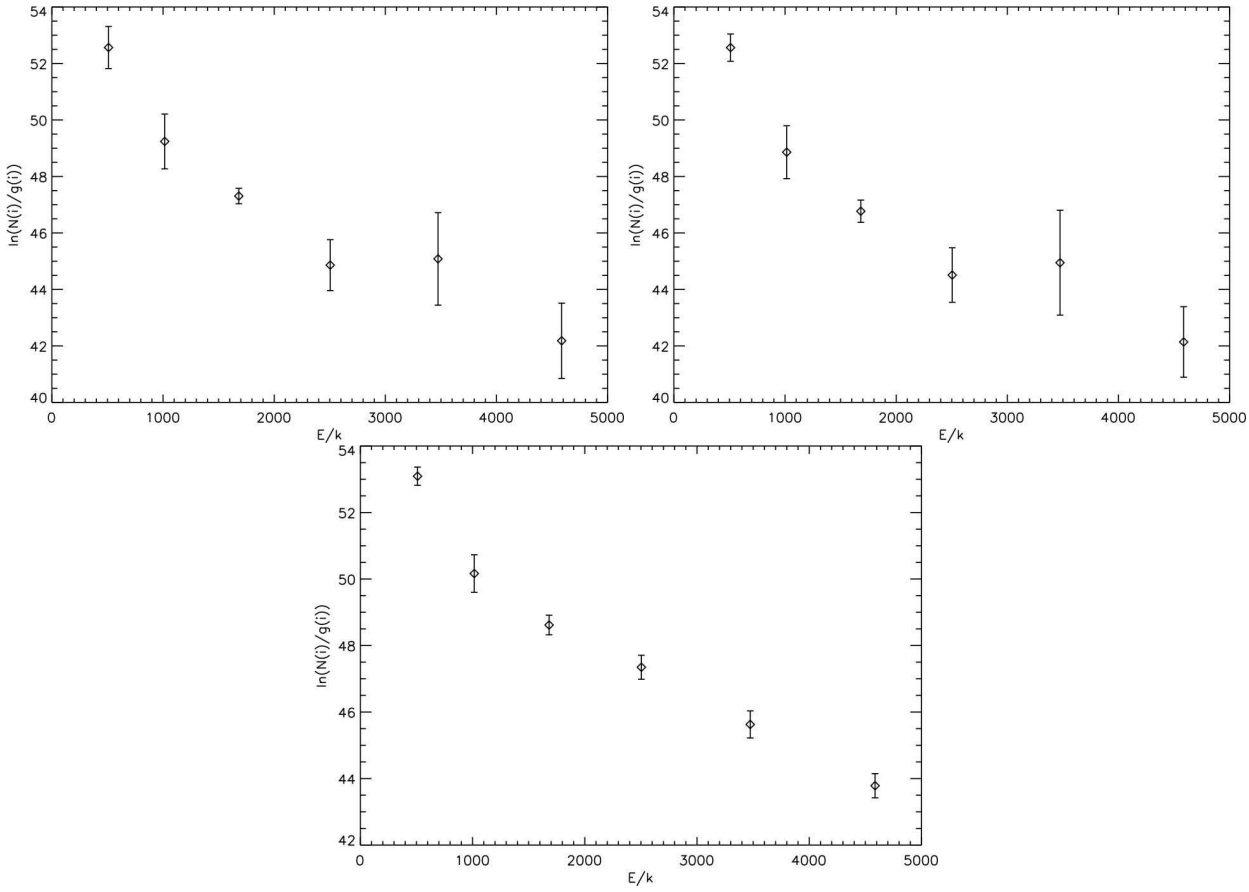

Fig. 2.— Excitation diagrams taken from 3 different regions along the M51 strip. The top two excitation diagrams are taken from regions within the southeast and northwest spiral arms that are 10.″2 in diameter (1.13×10^5 pc^2) and centered at (RA, Dec) of (202.45, 47.21) and (202.49, 47.18), respectively. The excitation diagram at the bottom is taken from from the nuclear region. The aperture is 10.″2 in diameter (1.13×10^5 pc^2), centered at (RA, Dec) of (202.47, 47.19).

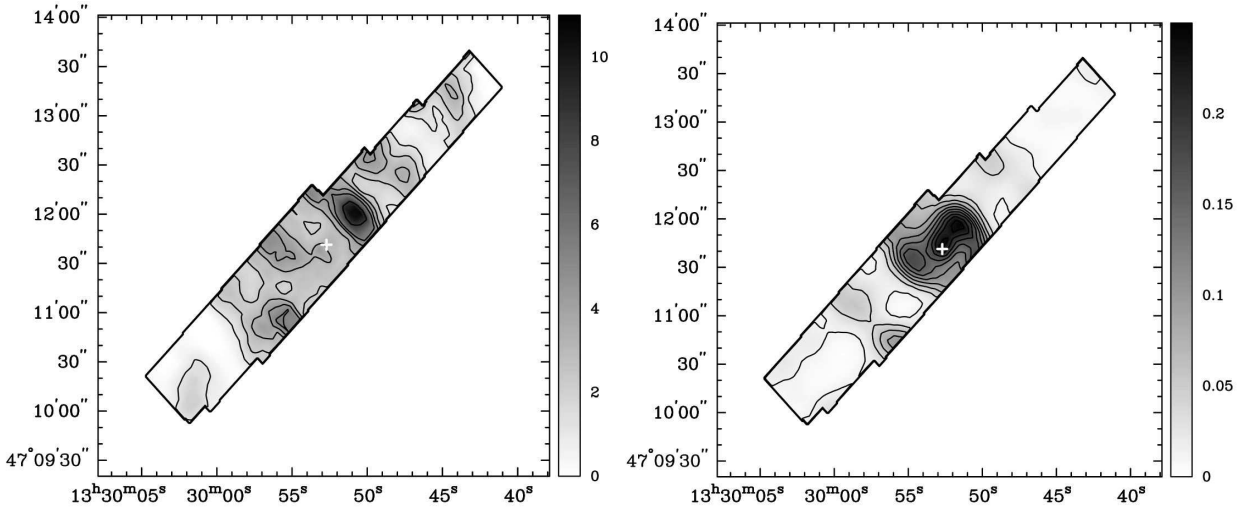

Fig. 3.— Shown are the warm (T = 100 − 300 K) H_2 (*left*) and hot (T = 400 − 1000 K) H_2 (*right*) mass distributions. The mass distributions are in units of $M_\odot/pc^2$. Contours are overplotted for clarity. The warm H_2 mass contour levels are at 8.85, 5.55, 4.43, 3.32, 2.21, and 1.10 $M_\odot/pc^2$. The hot H_2 contour levels are at 10 % of 0.25 $M_\odot/pc^2$. The hot H_2 mass distribution is derived from the fit to the H_2 S(2) − H_2 S(5) lines and the warm H_2 mass distribution is derived from the fit to the H_2 S(0) − H_2 S(2) lines, corrected for the contribution of the hot H_2 mass phase.

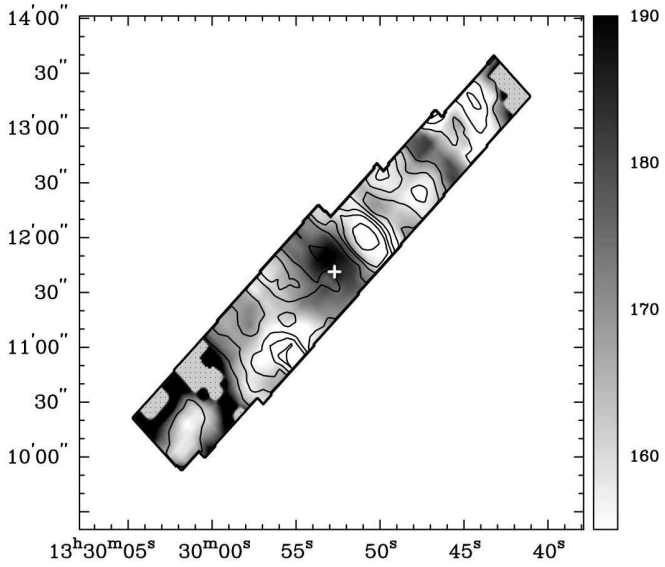

Fig. 4.— The warm (T = 100 − 300 K) H_2 mass distribution compared to the warm H_2 excitation-temperature. The warm H_2 excitation-temperature and mass distributions are derived from the fit to the excitation diagrams across the strip for the H_2 S(0) − H_2 S(2) lines, corrected for the contribution of the hot (T = 400 − 1000 K) H_2 phase. Mass density contour levels are at 8.85, 5.55, 4.43, 3.32, 2.21, and 1.10 $M_\odot/pc^2$ (same as in Figure **??**). The grey-scale represents the excitation-temperature distribution (in units of Kelvin). The non-rectangular shape to the map is due to the slight offset of the *Spitzer* IRS SL strip relative to the LL strip.

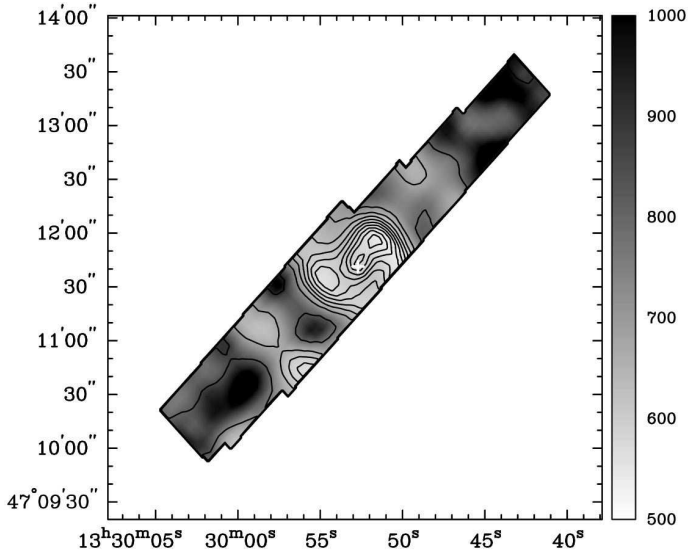

Fig. 5.— The hot (T = 400 − 1000 K) H_2 mass distribution compared to the hot H_2 excitation-temperature. The hot H_2 excitation-temperature and mass distributions are derived from the fit to the excitation diagrams across the strip for the H_2 S(2) − H_2 S(5) lines. Mass density contour levels are at 10% of 0.25 $M_\odot/pc^2$ (same as in Figure **??**). The grey-scale represents the excitation-temperature distribution (in units of Kelvin).

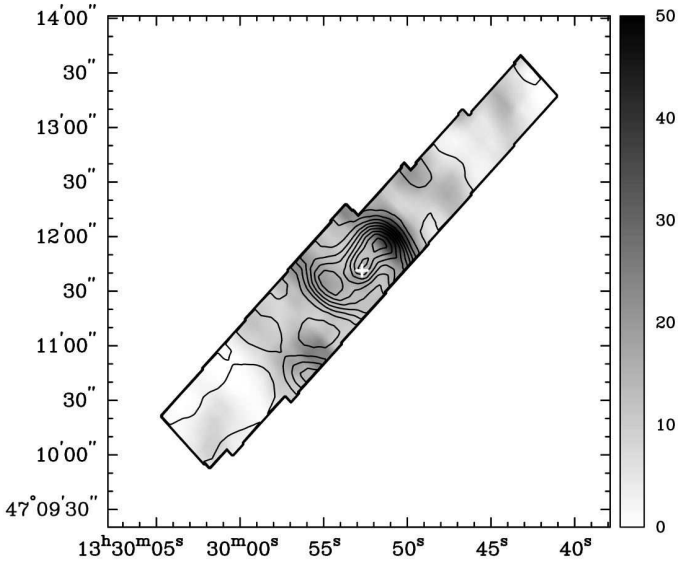

Fig. 6.— The warm (T = 100 − 300 K) H_2 mass (in grey-scale) compared to the hot (T = 400 − 1000 K) H_2 mass (in contours). Contours levels for the hot H_2 mass distribution are at 10% of the maximum mass density 0.25 $M_\odot/pc^2$. The grey-scale is in units of $M_\odot/pc^2$.

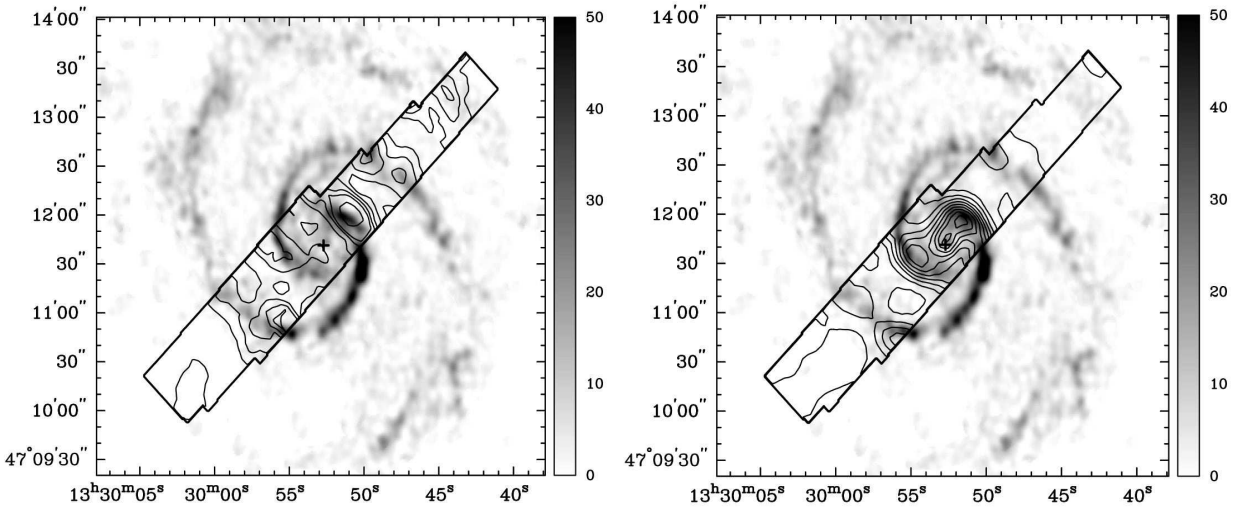

Fig. 7.— *Left*: Comparison of CO intensity (in grey-scale) to the warm (T = 100 − 300 K) H_2 mass (in contours). The CO intensity is in units of Jy beam s^{-1}. The warm H_2 mass contours are the same as in Figures **??** and **??**. *Right*: Comparison of CO intensity (in grey-scale) to the hot (T = 400 − 1000 K) H_2 mass (in contours). The CO intensity is in units of Jy beam s^{-1}. The hot H_2 mass contours are the same as in Figures **??** and **??**.

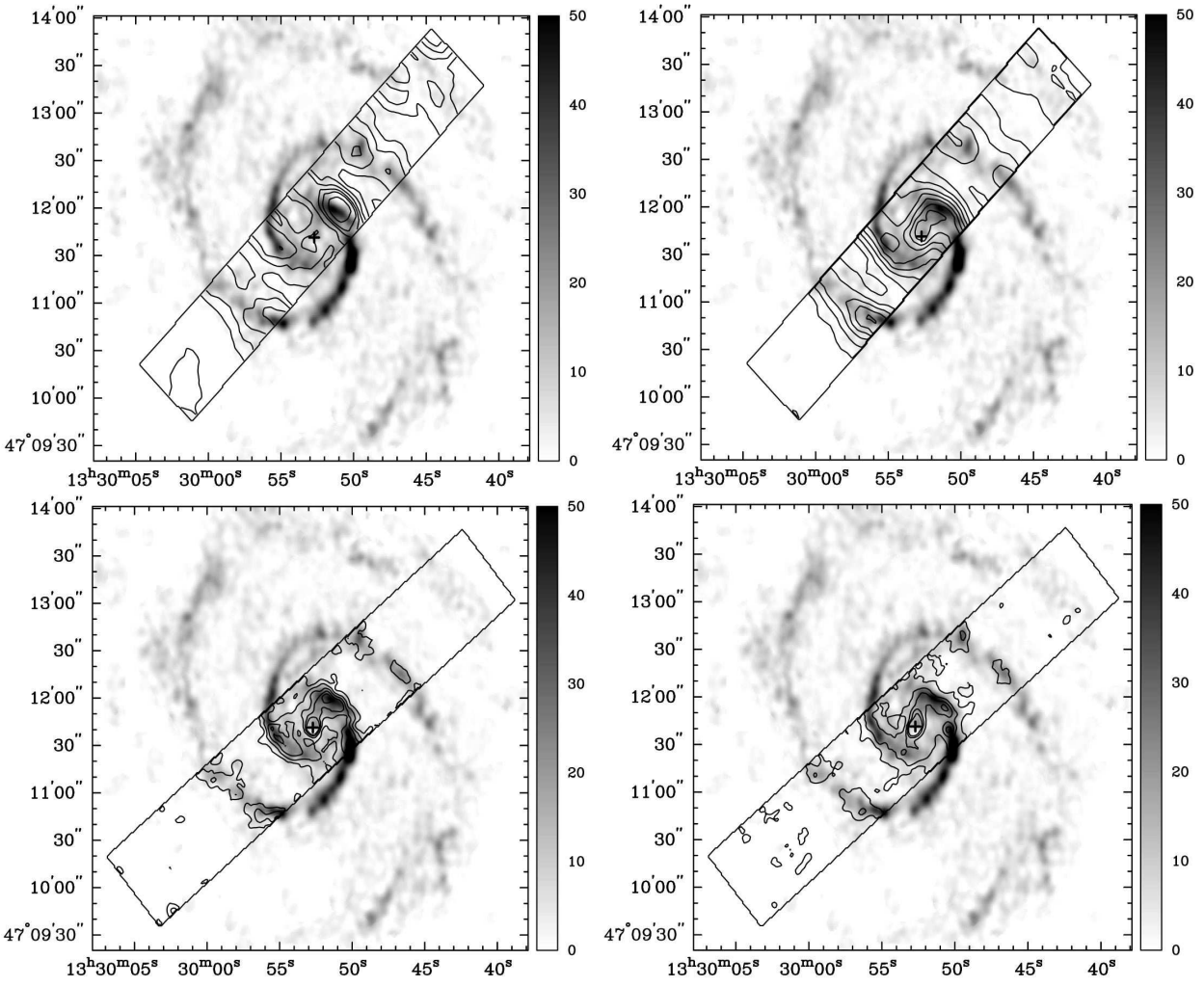

Fig. 8.— Comparison of the CO emission to the H_2 S(0) (*top left*), H_2 S(1) (*top right*), H_2 S(2) (*bottom left*), and H_2 S(3) (*bottom right*) emission. The CO emission maps are in units of Jy beam s^{-1}. Contour levels for H_2 S(0), H_2 S(1), H_2 S(2), and H_2 S(3) are the same as in Figure **??**.

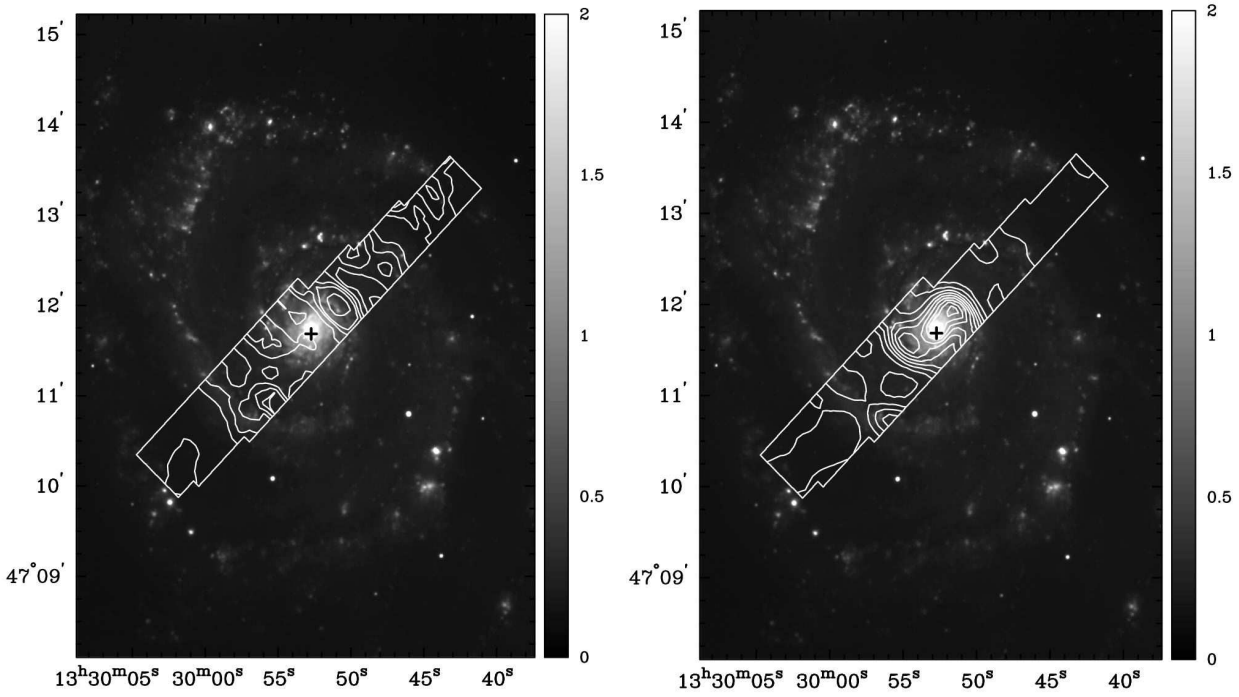

Fig. 9.— *Left*: Comparison of Hα (in grey-scale) to the warm (T = 100 − 300 K) H_2 mass (in contours). The Hα image is in units of counts/sec. The warm H_2 mass contours are the same as in Figures **??** and **??**. *Right*: Comparison of Hα (in grey-scale) to the hot (T = 400 − 1000 K) H_2 mass (in contours). The Hα image is in units of counts/sec. The hot H_2 mass contours are the same as in Figures **??** and **??**.

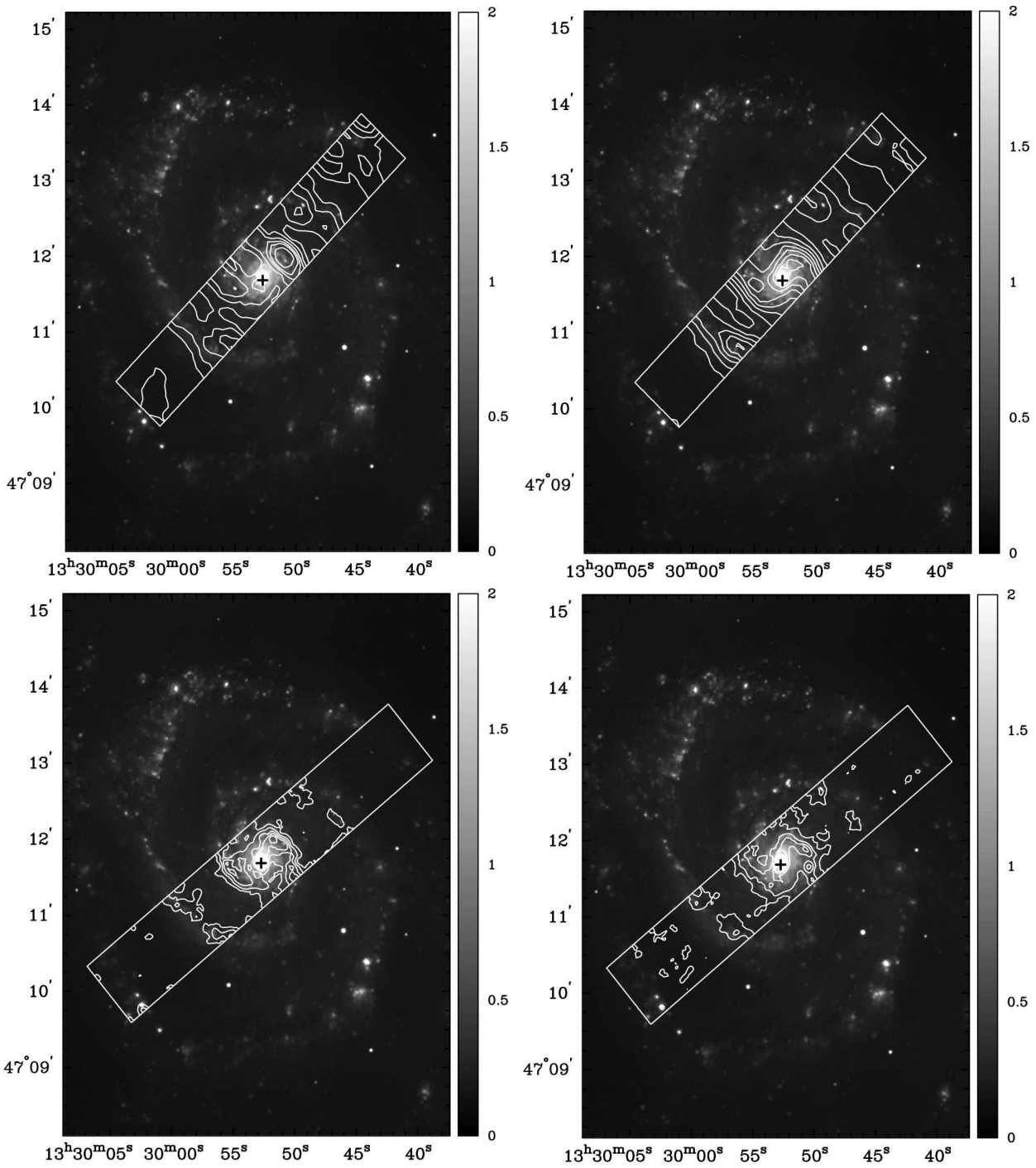

Fig. 10.— Comparison of Hα emission to the H_2 S(0) (*top left*), H_2 S(1) (*top right*), H_2 S(2) (*bottom left*), and H_2 S(3) (*bottom right*) emission. The Hα image is in units of counts/s. Contour levels for H_2 S(0), H_2 S(1), H_2 S(2), and H_2 S(3) are the same as in Figure **??**.

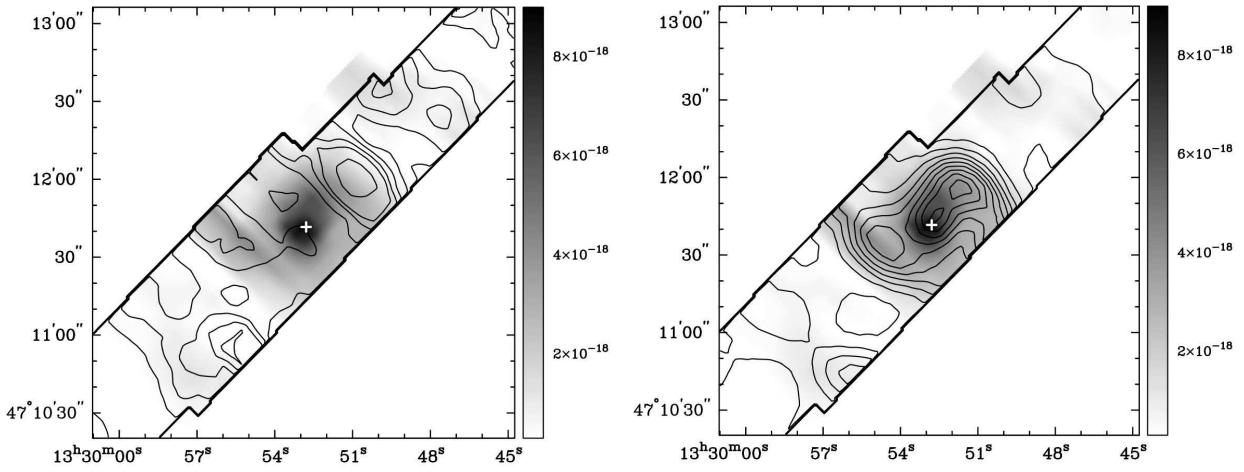

Fig. 11.— *Left*: Comparison of the [O IV](25.89 μm) emission (in grey-scale) to the warm (T = 100 K - 300 K) H_2 mass distribution (in contours). Hot H_2 mass contours are the same as in Figures **??** and **??**. *Right*: Comparison of the [O IV](25.89 μm) emission (in grey-scale) to the hot (T = 400 - 1000 K) H_2 mass distribution (in contours). Hot H_2 mass contours are the same as in Figures **??** and **??**. The [O IV](25.89 μm) emission is in units of W/m^2.

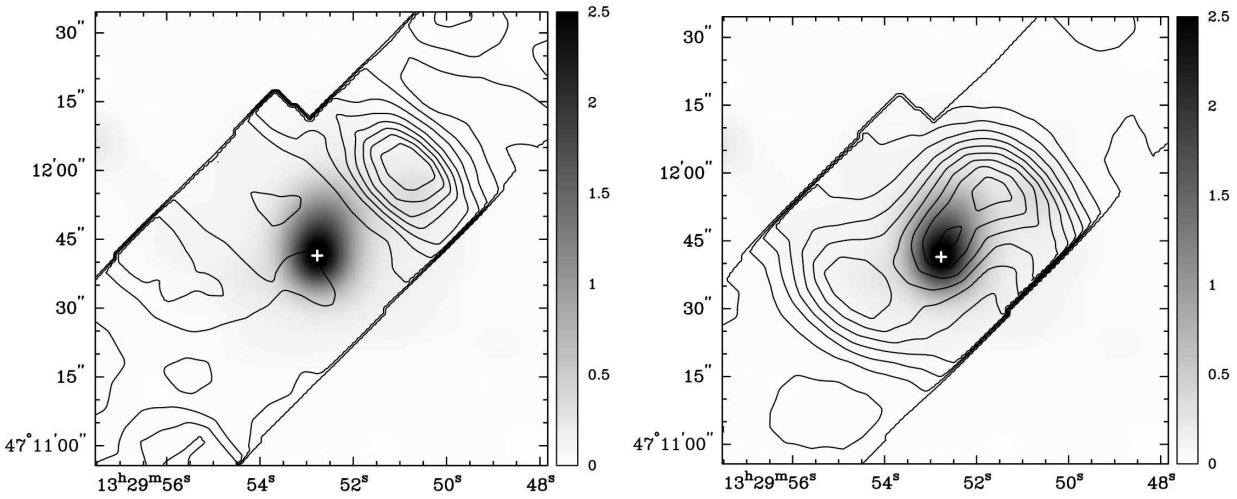

Fig. 12.— *Left*: Comparison of the smoothed 0.5 − 10 keV X-ray emission band (in grey-scale) to the warm (T = 100 − 300 K) H_2 mass distribution (in contours). The X-ray image has been smoothed to the same resolution as the warm H_2 mass map. X-ray emission is in units of counts. H_2 mass contours are the same as in Figures **??** and **??**. *Right*: Comparison of the smoothed 0.5 − 10 keV X-ray emission band (in grey-scale) to the hot (T = 400 − 1000 K) H_2 mass distribution (in contours). The H_2 mass distribution contours are the same as in Figures **??** and **??**.

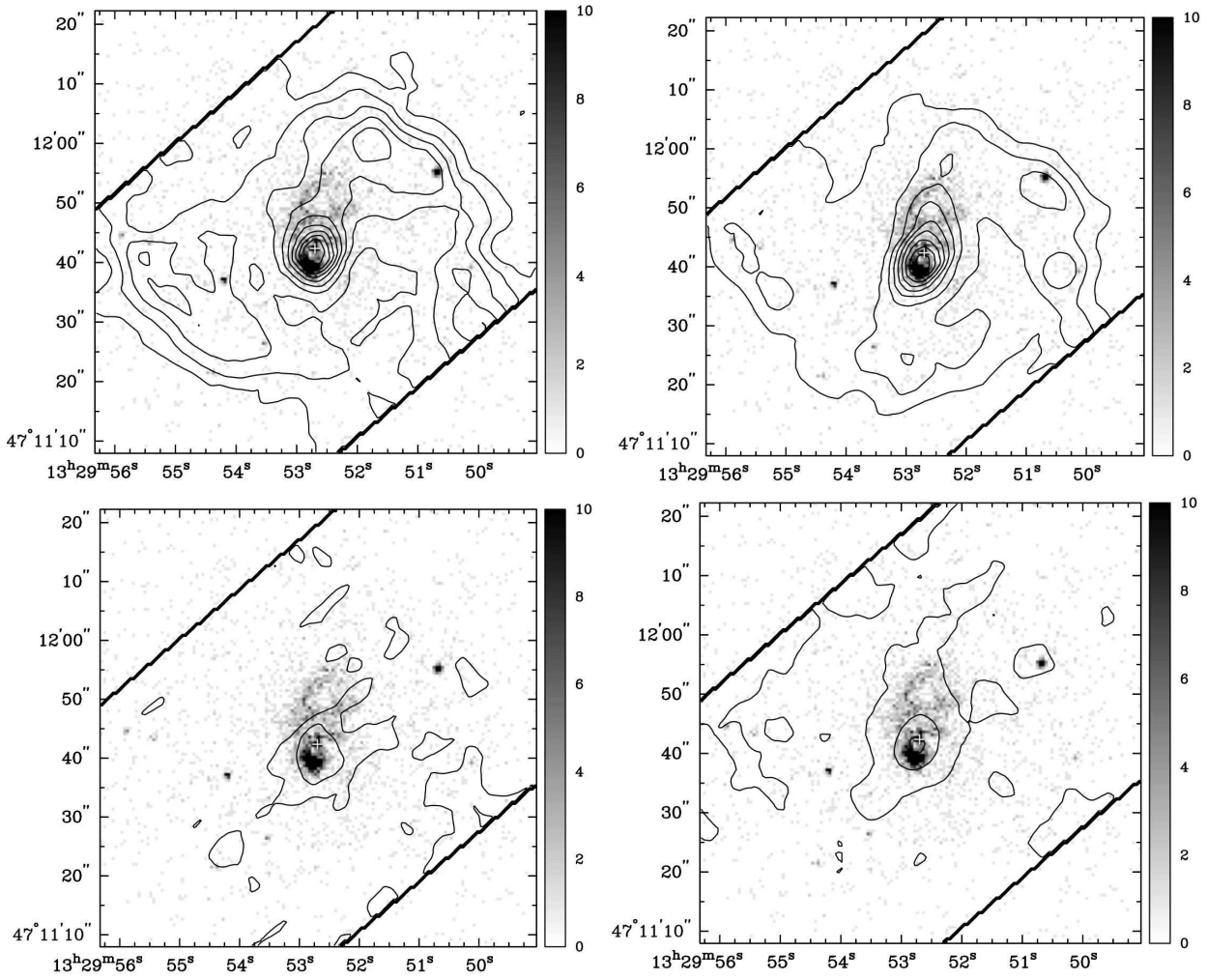

Fig. 13.— Comparison of the 0.5 − 10 keV X-ray emission band (in grey-scale) to the H_2 S(2) (*top left*), H_2 S(3) (*top right*), H_2 S(4) (*bottom left*), and H_2 S(5) (*bottom right*) emission in the nuclear region of M51. X-ray emission is in units of counts. The H_2 S(2) and H_2 S(3) emission contours are at 10 % of their peak values (2.20×10^{-18} and 1.35×10^{-17} W/m^2, respectively). The H_2 S(4) contours are at 2.0×10^{-18} and 1.0×10^{-18} W/m^2 and the H_2 S(5) contours are at 7.3×10^{-18}, 4.0×10^{-18}, and 8.0×10^{-19} W/m^2.

Table 1. H_2 Parameters

Transition	Wavelength (μm)	Rotational State (J)	Energy (E/k)	A (s^{-1})	Statistical Weight (g)
H_2(0-0)S(0)	28.22	2	510	2.94×10^{-11}	5
H_2(0-0)S(1)	17.04	3	1015	4.76×10^{-10}	21
H_2(0-0)S(2)	12.28	4	1682	2.76×10^{-9}	9
H_2(0-0)S(3)	9.66	5	2504	9.84×10^{-9}	33
H_2(0-0)S(4)	8.03	6	3474	2.64×10^{-8}	13
H_2(0-0)S(5)	6.91	7	4586	5.88×10^{-8}	45

Note. — The statistical weight (g) is $(2J+1)(2I+1)$ where I equals 1 for odd J transitions (ortho transitions) and I equals 0 for even J transitions (para transitions).